NON-EQUILIBRIUM SIMULATIONS OF FLUIDS UNDER THERMAL GRADIENTS: LOCAL PROPERTIES AND COUPLING EFFECTS

Fernando Bresme[1,2]

[1] Department of Chemistry, Imperial College London, SW7 2AZ, United Kingdom
[2] Department of Chemistry, Norwegian University of Science and Technology (NTNU), Trondheim, NO-7491, Norway
*f.bresme@imperial.ac.uk

ABSTRACT

External fields drive fascinating non-equilibrium phenomena in solutions. Ludwig [1] and later Soret [2] reported such phenomena in aqueous solutions. Thermal gradients induce induce mass separation, thermodiffusion, with the salt and water migrating towards hot or cold regions. Recent experiments have considered more complex fluids such as polymers and biomolecules (thermophoresis) [3; 4; 5; 6], and very recently it was shown that thermal gradients induce Casimir-like forces between plates that are maintained at different temperatures [7]. In addition to fundamental questions, thermal coupling effects are relevant in practical applications [8].

The thermodiffusion and thermophoresis effects are very sensitive to the temperature of the system, and small changes in temperature can induce the drift of the solute to hot or cold regions. There has been considerable effort in developing a theory to predict the thermal response of solutions [9; 10; 11], however a full predictive theory is still an outstanding objective.

In this contribution I discuss recent work that illustrates how non-equilibrium computer simulations can be used to investigate fundamental questions concerned with systems away from equilibrium, and how simulations can be used to uncover coupling effects in molecular fluids when they are exposed to thermal gradients.

Simulating Thermal Gradients

Computer simulations have expanded considerably the scope of theoretical approaches to investigate non-equilibrium phenomena. Non-equilibrium molecular dynamics simulations (NEMD) provides a powerful tool to study thermodiffusion and thermophoresis. Since the introduction of non-equilibrium methods in the 1970's, several improvements to treat fluids under thermal gradients have been implemented over the years [12].

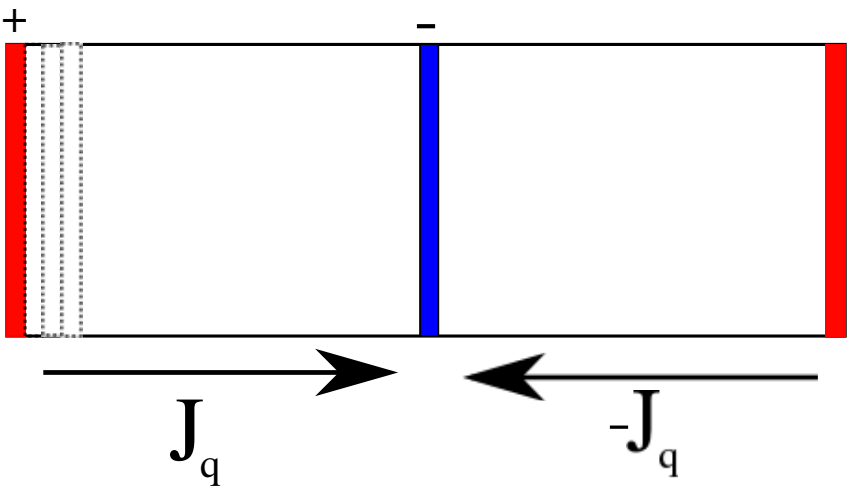

Figure 1: Simulation set up employed to perform non-equilibrium simulations under thermal gradients. The red and blue regions represent the hot and cold termostats, respectively. J_q is the heat flux. The dashed lines represent an example of 3 subvolumes that are used to compute local properties.

Figure 1 shows one implementation of NEMD to simulate thermal gradients, which has been widely used in NEMD simulations [13; 14; 15; 16] as the simulation can be performed using full periodic boundary conditions. Two thermostats are implemented in the simulation box. One in the middle of the box where particles are thermostatted at a temperature T_1, and another one at the edges of the box, where the particles are themostatted at temperature $T_2 > T_1$ (see Figure 1). The thermostatting is performed conserving the momentum of the system. The coordinates do not change between thermostatting events, and the change in kinetic energy is equal to the change in internal energy between thermostatting events. The use of thermostats offers advantages, as the temperature range to be investigated in the non-equilibrium simulations can be defined exactly. The kinetic energies at the thermostats can be adjusted using simple velocity rescaling, where the old velocities are reset to, $\mathbf{v}_{i,new} = \chi \mathbf{v}_{i,old}$, with $\chi = \sqrt{K_t/K_{old}}$ being the ratio of the "old" and "target" temperatures. More sophisticated canonical thermostats have also been employed. The results are fairly insensitive to the thermostat used. The method shown in Figure 1 induces two heat fluxes that act in opposite direction. The average heat flux can be obtained using the statistical mechanics equation derived by Irving and Kirkwood [17] or from from the continuity equation,

$$J_q = \frac{\Delta U}{2\delta t A} \tag{1}$$

where ΔU is the average change of internal energy (kinetic energy) in the thermostatting process, δt is the simulation time step and A the cross sectional area of the simulation box. The heat flux can then be used to compute the thermal conductivity via Fourier's law, $\lambda = -J_q/\nabla T$.

The thermal gradients employed in NEMD simulations are in general rather large, $\sim 10^{10}$ K/m. This is necessary to reduce the impact of thermal fluctuations, and to increase the signal to noise ratio. Despite the large thermal gradients the response of the fluids to the thermal gradients remains in the linear regime. For fluids the characteristic length scale for heat transport, a, is rather short, about one molecular diameter. Hence, $\nabla T T^{-1} a << 1$, showing that the thermal transport is defined mostly in the diffusive regime.

The definition of temperatures under non-equilibrium conditions has motivated a number of works (see reference [18] for an in depth discussion). NEMD allows testing the consistency of kinetic and configurational definitions [19; 20; 21; 22]. Figure 2 shows temperature profiles for Lennard-Jones fluids at high density (average density $\bar{\rho} = 0.7$ in reduced units). NEMD simulations show that the configurational (conF) and kinetic (kin) routes are fully consistent, within the numerical accuracy of our computations, at conditions away from equilibrium. Figure 2 also shows that some definitions can introduce large errors [22]. These discrepancies are connected to the large dependence of some of these temperatures (con1 in Figure 2) with system size. This strong dependence becomes very important when the sampling volume is very small (see subvolumes employed in NEMD simulations in Figure 1).

One advantage of non-equilibrium simulations is the possibility of computing local properties. This notion is also illustrated in Figure 2, which shows the thermal conductivity extracted from the *local* temperature gradients. The agreement between the configurational and kinetic route (conF and kin) is excellent. The comparison with equilibrium data obtained from the Green-Kubo relation is also in excellent agreement, showing that the notion of local equilibrium is supported by computations of *local* transport properties.

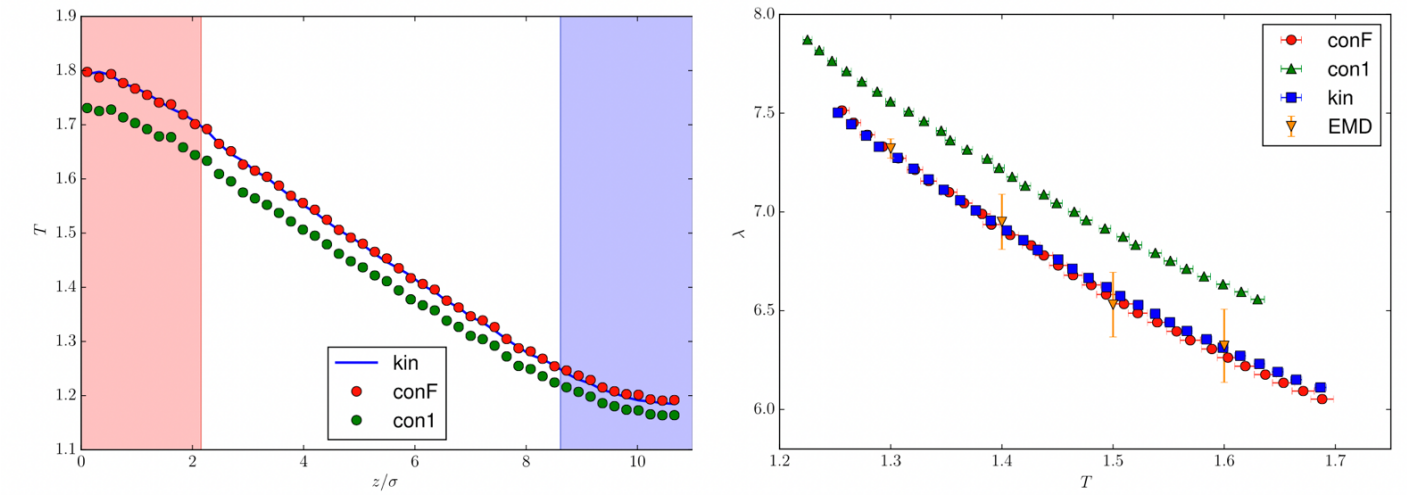

Figure 2: (Left) Temperature profiles for obtained with kinetic and configurational temperatures. The red and blue areas represent the position of the thermostats. (Right) Thermal conductivity calculated from Fourier's law using local thermal gradients from the profiles represented on the left. EMD data refer to thermal conductivities obtained from the Green-Kubo equations. The Lennard-Jones potential cutoff is 5σ, where σ is the atom diameter. Figures adapted from reference [22].

Coupling effects under thermal gradients

In addition to the well known thermodiffusion effects mentioned above, thermal gradients can induce coupling non-equilibrium effects in pure molecular fluids. These effects can be illustrated with model fluids consisting of dumbbells with anisotropy in size and/or mass [23]. The coupling of the internal degrees of freedom with the heat flux induces a preferred orientation in the fluid. Non-Equilibrium Thermodynamics (NET) provides a route to rationalize this physical behaviour [23]. The energy needed to maintain a given orientation, defined by the vector $\vec{n}$ (see Figure 3), is given by $E = k \langle \vec{n} \rangle^2 /2$, where k is a force constant. The corresponding inear flux-force relations are given by,

$$\frac{\partial \langle \vec{n} \rangle}{\partial t} = -\frac{L_{nn}}{T} k \langle \vec{n} \rangle - \frac{L_{nq}}{T^2} \vec{\nabla} T \tag{2}$$

$$\vec{J}_q = -\frac{L_{qn}}{T} k \langle \vec{n} \rangle - \frac{L_{qq}}{T^2} \vec{\nabla} T \tag{3}$$

where $L_{\alpha\beta}$ are the phenomenological coefficients and $L_{nq} = L_{qn}$. For the stationary state, $\partial \langle \vec{n} \rangle /\partial t = 0$, and we get [23],

$$\langle \vec{n} \rangle = -C \frac{\nabla T}{T} \tag{4}$$

where $C = L_{nq}/(k L_{nn})$.

Figure 3 shows simulation results that confirm the existence of the *thermal orientation* effect in dumbbells consisting of particles with the same mass but different size, $\sigma_{22}/\sigma_{11} = 1/2$. The NEMD simulation results agree with the NET predictions. The orientation of the fluid increases linearly with the strength of the thermal gradient (see ref. [23]) as predicted by equation (4). The orientation is also sensitive to the thermodynamic conditions. The orientation is stronger at higher/lower packing fractions/temperatures. The dependence of the orientation with the thermodynamic conditions cannot be inferred from the NET approach. These coupling effects can be extended to situations were more that one external field, *e.g.* thermal and gravitational, is applied to the system [24].

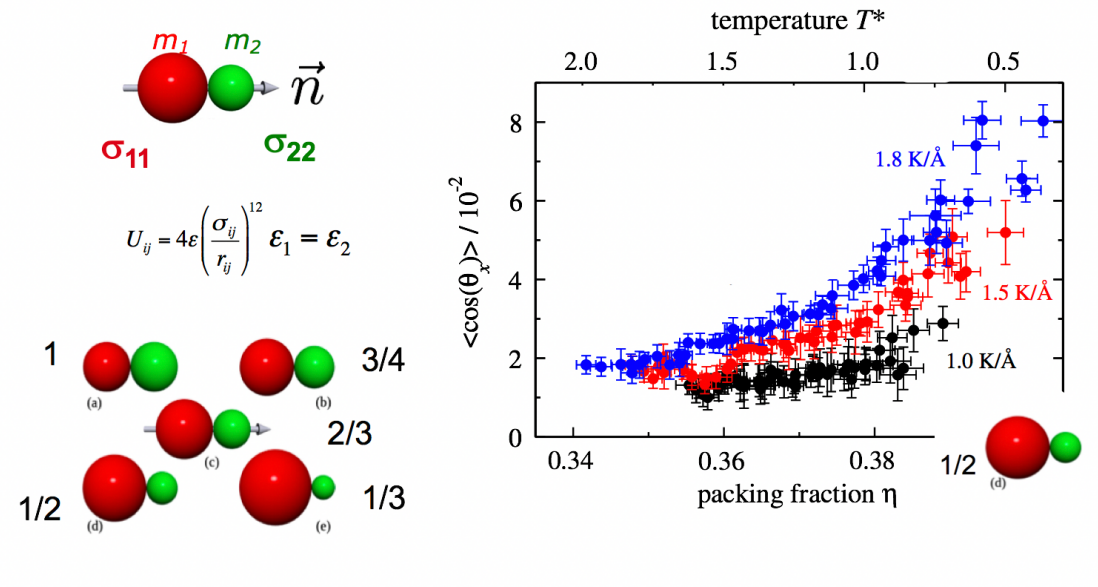

Figure 3: (Left) Sketch of dumbbell molecules consisting of tangent spheres of different mass and/or size. The equation shows the pair interaction between the dumbbell sites in different molecules. The arrow denotes the direction of the vector $\vec{n}$, which defines the orientation of the molecules. (Right) Dependence of the orientation induced by three different thermal gradients with the packing fraction or temperature. Figures adapted from reference [23].

The coupling of internal degrees of freedom with heat fluxes is particularly interesting in polar fluids, such as water, since the thermal gradient induces an electrostatic field. Using a non-equilibrium treatment similar to the one discussed above for dumbbells, it is possible to derive an equation that predicts the electrostatic field, **E**, as a function of the thermal gradient strength [25],

$$\mathbf{E} = \left(1 - \frac{1}{\varepsilon_r}\right)\frac{L_{pq}}{L_{pp}}\frac{\nabla T}{T} = S_{TP}\nabla T \tag{5}$$

where $L_{\alpha\beta}$ represent again phenomenological coefficients, ε_r is the permittivity of the solvent and S_{TP} is the Thermo-Polarization coefficient. Equation (5) is similar to the equation defining thermoelectric effects in terms of the Seebeck coefficient [26].

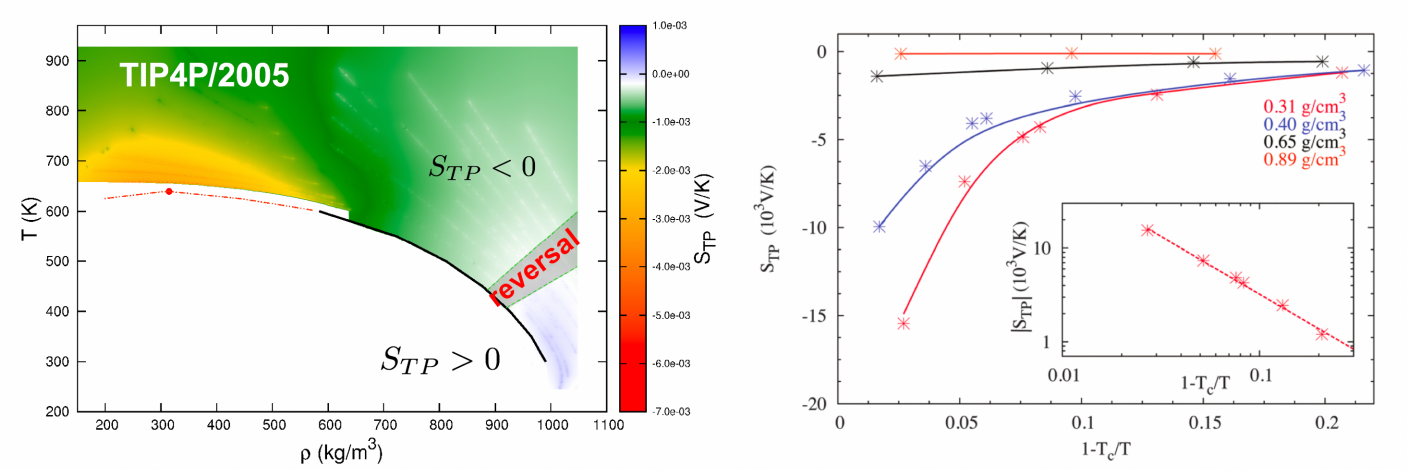

Figure 4: (Left) Variation of the thermo-polarization (TP) coefficient in TIP4P-2005 water as a function of temperature and density. The white region corresponds to coexistence conditions. The full and dashed lines represent the coexistence line, and the filled circle is an estimate of the critical point of TIP4P/2005 water. The "reversal" region indicates the area of the temperature/density plane where the TP coefficient changes sign. The color scale shows the magnitude of the TP effect (see scale on the right of the figure). (Right) Variation of the TP coefficient along different isochores, including the critical one (0.31 g/cm^3). The inset shows the dependence of the coefficient (in absolute value) with the distance to the critical point, $1 - T_c/T$. The dashed line represent a fitting to the equation $|S_{TP}| = (1 - T_c/T)^{-\gamma}$ using $\gamma = 1.239$. Figures adapted from reference [16].

NEMD simulations can be used to compute the coefficient S_{TP} and therefore the strength of the TP effect. The variation of the magnitude and sign of this coefficient is complex, changing sign from low to high temperatures. The sign of the coefficient is defined by the balance of dipolar and quadrupolar contributions to the electrostatic field of water. The quadrupolar term depends on the thermal expansion fairly strongly and dominates the TP response at high temperatures [27].

The thermal polarization increases significantly upon approaching a critical point. This effect is connected to the increase of the thermal expansion, and the eventual divergence of this property. The increase of the polarization response along the critical isochore can be described with the equation, $|S_{TP}| = (1 - T_c/T)^{-\gamma}$ [16]. This equation describes the dependence of other properties (e.g. compressibility or thermal expansion) with temperature, as the system approaches the critical point. The exponent $\gamma = 1.239$, which corresponds to the universality class of Ising-like systems (such as water), describes well the simulation results and the increase of the TP coefficient as the critical point is approached.

NEMD simulations predict an interesting physical behaviour near critical conditions , where small thermal gradients could induce a significant polarization in water. As a reference we find that strong thermal gradients 10^{6-8} K/m, which can be generated easily at the nanoscale using metallic nanoparticles, could induce fields equivalent to 10^{4-6} V/m. Such predictions await experimental verification. Light scattering techniques could be helpful to advance in an experimental study of these non-equilibrium phenomena.

Acknowledgments

I would like to thank Jeff Armstrong, Dick Bedeaux, Signe Kjelstrup, Anders Lervik, Miguel Rubí and Jan Sengers for many discussions over the years and for fruitful collaborations. Also I would like to thank Jan Sengers for interesting discussion on Light Scattering experiments. I thank the EPSRC (EP/J003859/1) and the Research Council of Norway (Project 221675) for financial support and the Imperial College High Performance Computing Service for providing computational resources.

REFERENCES

[1] C. Ludwig, *Sitz. ber. Akad. Wiss. Wien Math.-Nat. wiss. Kl*, 539, **50** (1856).
[2] C. Soret, *Arch. Sci. Phys. Nat.*, Geneve, 48, **2** (1879).
[3] S. Wiegand, *J. Phys.: Condens. Matter*, R357, **16** (2004).
[4] R. Piazza and A. Parola, *J. Phys.: Condens. Matter*, 153102, **20** (2008).
[5] S. Putnam, D. Cahill and G. Wong, *Langmuir*, 9221, **23** (2007).
[6] M. Reichl, M. Herzog, A. Götz and D. Braun, *Langmuir*, 9221, **23** (2007).
[7] T. Kirkpatrick, J.O. de Zarate and J.V. Sengers, *Phys. Rev. Lett.*, **115**, 035901 (2015).
[8] P. Baaske, F. Weinert, S. Duhr, K. Lemke, M. Russel, and D. Braun, *Proc. Natl. Acad. Sci. USA*, **104**, 9346 (2007).
[9] S. Duhr and D. Braun, *Phys. Rev. Lett.*, **96**, 168301 (2006).
[10] C. Debuschewitz and W. Köhler, *Phys. Rev. Lett.*, **87**, 055901 (2001).
[11] K. Eslahian, A. Majee, M. Maskos, and A. Würger, *Soft Matter*, **10**, 1931 (2014).
[12] F. Bresme, A. Lervik and J. Armstrong, *Non-equilibrium Molecular Dynamics*, Chapter 6, in Experimental Thermodynamics Volume X: Non-Equilibrium Thermodynamics with Applications, D. Bedeaux, S. Kjelstrup and J.V. Sengers eds., IUPAC, p. 105 (2016).
[13] A. Tenenbaum, *Phys. Rev. A*, **28**, 3132 (1983).
[14] B. Hafskjold, in Thermal Nonequilibrium Phenomena in Fluid Mixtures, Lecture Notes in Physics, ed. W. Köhler and S. Wiegand, Springer, p. 3, (2001).
[15] F. Müller-Plathe, *J. Chem. Phys.*, **106**, 6082 (1997).
[16] I. Iriarte-Carretero, M.A. Gonzalez, J. Armstrong, F. Fernandez-Alonso and F. Bresme, *Phys. Chem. Chem. Phys.*, 19894, **18** (2016).
[17] J. H. Irving and J. G. Kirkwood, *J. Chem. Phys.*, 817, **18** (1950).
[18] J. Casas-Vázquez J and D. Jou, *Rep. Prog. Phys.*,1937 **66** (2003).
[19] H.H. Rugh, *Phys. Rev. Lett.*, 772, **78** (1997).
[20] O. Jepps, G. Ayton and D. Evans, *Phys. Rev. E.*, **62**, 4757 (2000).
[21] A. Lervik A, O. Wilhelmsen, T.T. Trinh and H.R. Nagel, *J. Chem. Phys.*, 114106, **143** (2015).
[22] N. Jackson, J. M. Rubi and F. Bresme, Mol. Sim., 1214, **42** (2016).
[23] F. Römer, F. Bresme, J. Muscatello, D. Bedeaux and J.M. Rubi, *Phys. Rev. Lett.*, 105901 **108** (2012).
[24] C.D. Daub, J. Tafjord, S. Kjesltrup, D. Bedeaux and F. Bresme, *Phys. Chem. Chem. Phys.*, 12213, **18** (2016).
[25] F. Bresme, A. Lervik, D. Bedeaux and S. Kjelstrup, *Phys. Rev. Lett.*, 020602 **101** (2008).
[26] S.R. de Groot and P. Mazur P., Non-equilibrium thermodynamics, New York, Dover, (1984).
[27] J. Armstrong and F. Bresme, *Phys. Rev. E*, 060103, **92** (2015).